LAVA HyperSense and deep-learning reconstruction for near-isotropic (3D) enhanced magnetic resonance enterography in patients with Crohn's disease: utility in noise reduction and image quality improvement

Jung Hee Son 🔾
Yedaun Lee 🔾
Ho-Joon Lee 🔾
Joonsung Lee 🔾
Hyunwoong Kim 🔾
Marc R. Lebel 🔾

PURPOSE
This study aimed to compare near-isotropic contrast-enhanced T1-weighted (CE-T1W) magnetic resonance enterography (MRE) images reconstructed with vendor-supplied deep-learning reconstruction (DLR) with those reconstructed conventionally in terms of image quality.

METHODS
A total of 35 patients who underwent MRE for Crohn's disease between August 2021 and February 2022 were included in this retrospective study. The enteric phase CE-T1W MRE images of each patient were reconstructed with conventional reconstruction and no image filter (original), with conventional reconstruction and image filter (filtered), and with a prototype version of AIR™ Recon DL 3D (DLR), which were then reformatted into the axial plane to generate six image sets per patient. Two radiologists independently assessed the images for overall image quality, contrast, sharpness, presence of motion artifacts, blurring, and synthetic appearance for qualitative analysis, and the signal-to-noise ratio (SNR) was measured for quantitative analysis.

RESULTS
The mean scores of the DLR image set with respect to overall image quality, contrast, sharpness, motion artifacts, and blurring in the coronal and axial images were significantly superior to those of both the filtered and original images ($P < 0.001$). However, the DLR images showed a significantly more synthetic appearance than the other two images ($P < 0.05$). There was no statistically significant difference in all scores between the original and filtered images ($P > 0.05$). In the quantitative analysis, the SNR was significantly increased in the order of original, filtered, and DLR images ($P < 0.001$).

CONCLUSION
Using DLR for near-isotropic CE-T1W MRE improved the image quality and increased the SNR.

KEYWORDS
Crohn's disease, MR enterography, image quality, deep learning, noise reduction

From the Department of Radiology (J.H.S., Y.L. ✉ chosai81@gmail.com, H-J.L.), Inje University College of Medicine, Haeundae Paik Hospital, Busan, Republic of Korea; GE Healthcare Korea, Seoul, Republic of Korea (J.L.); Clinical Trial Center (H.K.), Inje University College of Medicine, Haeundae Paik Hospital, Busan, Republic of Korea; GE Healthcare Canada (M.R.L.), Calgary, Canada.

Crohn's disease (CD) is a chronic bowel inflammatory disease characterized by transmural discontinuous asymmetric inflammation that affects the bowel wall and is frequently accompanied by extramural complications.[1,2] Cross-sectional imaging plays an important role in CD diagnosis and monitoring. As CD often presents in young populations who require repeat imaging during their lifetimes,[3,4] magnetic resonance enterography (MRE) is preferred because of its high-contrast resolution, multiple imaging parameters, and lack of ionizing radiation.[5-7]

Contrast-enhanced T1-weighted (CE-T1W) coronal imaging is a key component of MRE for evaluating the extent and severity of bowel inflammation.[8-10] CE-T1WCE-T1W coronal dynamic images are acquired using ultrafast spoiled gradient-echo (GRE) sequences with fat suppression. Currently, three-dimensional (3D) volumetric imaging techniques allow us to obtain near-isotropic dynamic images that provide high-spatial-resolution images with a relatively short total acquisition time. As the pixels are nearly isotropic, 3D datasets can easily be reformatted in any plane without loss of image resolution and demonstrate fine anatomic detail with thin sections.[11] However, owing to bowel peristalsis or respiration and limited breath-holding duration, it is challenging to obtain high-resolution isotropic images without compromising image quality.

Compressed sensing (CS) enables near-isotropic CE-T1W coronal images to be obtained within a short scan time with a single-breath hold.[12,13] It can also be useful for reducing noise. However, blurring can be introduced when the images are not sufficiently compressible or when excessive acceleration is used. Additionally, when the scan time is fixed for acquiring high-resolution images, the signal-to-noise ratio (SNR) can be decreased as a tradeoff between the SNR and resolution.[14] Recent advances in MR imaging (MRI) technology have introduced deep learning to the image reconstruction process, which, in this study, was expected to improve the SNR and image sharpness compared with CS alone.[15]

However, the utility of deep learning to reduce noise and improve sharpness for MRE has not yet been investigated. Therefore, the purpose of this study was to compare near-isotropic CE-T1W images of MRE reconstructed using deep-learning reconstruction (DLR), conventional reconstruction, and image filter (filtered) techniques as well as conventional reconstruction and no image filter (original) in terms of image quality.

Methods

This retrospective single-center study was approved by the Inje University Haeundae Paik Hospital Institutional Review Board Ethics Committee (protocol number: HPIRB 2022-04-028-001) on April 28, 2022, and the requirement for informed consent was waived.

Study population

We retrospectively registered consecutive patients with known or suspected CD who underwent MRE at our institution between August 2021 and February 2022. In total, 36 patients were identified; one was excluded because of severe degradation of image quality, and 35 patients were included in the final analysis. Patient demographics and CD-related patient characteristics at the time of MRE were collected from electronic medical records.

MRE protocol

After the oral administration of 1.000 mL of polyethylene glycol solution (Coolprep, Taejoon Pharmaceutical Co.), MRE was performed. Scans were acquired using a 3 T MRI scanner (SIGNA™ Architect, GE Healthcare) with two 30-channel surface coils (AIR™ anterior array coils). To avoid bowel peristalsis, 7.5 mg of cimetropium bromide (Alpit, Hana Pharmaceutical Co.) was administered at three different intervals during the examination; the first dose was administered just before the start of the scan, the second dose was administered just before the diffusion-weighted image was obtained, and the third dose was administered just before the coronal T1-weighted images were obtained. The coronal T1-weighted spoiled GRE sequence [liver acquisition with acceleration volume acquisition (LAVA)] with fat suppression was acquired during breath-holding, before contrast injection, and at enteric and portal phases that were obtained after the intravenous administration (0.2 mL/kg at a rate of 2 mL/s) of gadoterate meglumine (Dotarem, Guerbet) followed by a saline bolus injection. A coronal enteric phase was obtained using bolus tracking when the contrast material arrived at the abdominal aorta. The coronal portal phase image was subsequently obtained after providing breath-holding instructions between the two phases. The typical imaging parameters of the fat-suppressed LAVA in this study are summarized in Table 1. The scan time was set to approximately 17 seconds, with slight variations made to accommodate the patient's size.

Three image sets of enteric phases were generated: one with conventional reconstruction and no image filter (original), one with conventional reconstruction and vendor-provided image filter (B, high sharpening, some smoothing) (filtered), and one with a vendor-supplied prototype of AIR™ Recon DL 3D (DLR).[16,17] The DLRs were performed offline using an Intel (Santa Clara, CA) Core i7-10850H CPU (2.70 GHz and six cores), which took approximately one hour to complete each series. These image sets were then reformatted into an axial plane with a slice thickness of 1.4 mm.

In our institution, the filtered image is a standard-of-care (SOC) 3D reconstructed im-

Main points

- Deep learning in reconstruction (DLR) can improve image quality and increase the signal-to-noise ratio in contrast-enhanced T1-weighted (CE-T1W) magnetic resonance enterography (MRE).

- The DLR technique enables high-resolution near-isotropic CE-T1W MRE with diagnostic image quality.

- Near-isotropic CE-T1W MRE allows high-quality axial reformatted images to be obtained from the same dynamic phase, which is useful for the multiplanar evaluation of anatomical details of bowel segments or extramural complications of Crohn's disease.

Table 1. Scan parameters for coronal T1-weighted spoiled gradient-echo sequence (liver acquisition with acceleration volume acquisition) with fat suppression for the magnetic resonance enterography protocol in this study

Parameter	Value
Orientation	Coronal
TR/TE (ms/ms)	3.6/1.6
FOV (mm)	380 x 304
No. of slices	120
Bandwidth (kHz/pixel)	83.33
Matrix	300 x 260
Voxel size (mm³)	1.3 x 1.5 x 1.6
Flip angle (degrees)	10
Fat saturation	SPECIAL
Acceleration factor	2 x 1.8
HyperSense factor	1.2

SPECIAL, spectral inversion at lipid; TR, repetition time; TE, echo time; FOV, field of view

age that uses a postprocessing filter after the image is reconstructed. The filter is applied as a postprocessing step after image reconstruction and works by trading-off noise reduction and image sharpening in the image domain. Specifically, the filter employs smoothing to reduce noise, which can cause the image to appear blurred, and image sharpening to enhance the clarity of the image, which can increase the noise level.

AIR™ Recon DL is a deep-learning-based reconstruction method for improving image sharpness by removing truncation artifacts while jointly denoising the image to improve its quality.[16-18] It applies a convolutional neural network (CNN) in an image-reconstruc-tion pipeline using raw k-space data to generate high-fidelity images. The CNN is trained in a supervised manner to generate high-resolution data with minimal ringing artifacts and very low noise levels.[16] The AIR™ Recon DL, which was originally designed for 2D imaging, was extended to 3D to reduce noise and ringing in all three directions, thus improving both SNR and spatial resolution.[17,18] The vendor-provided AIR™ Recon DL 3D prototype was applied offline to the raw k-space data following image acquisition. The prototype DLR allowed for tunable noise-reduction levels (25%, 50%, and 75%, with higher levels corresponding to greater denoising). After conducting phantom experiments and reaching a consensus during preliminary reading sessions, the denoising level was selected at 75% based on agreement among the readers (Supplementary Figures 1, 2).

Image analysis

Two abdominal radiologists (J.H.S. and Y.L., with 8 and 15 years of experience in interpreting MRE, respectively) independently assessed each coronal and reformatted axial image of three image sets (original, filtered, and DLR) for subjective image quality using a 5-point Likert scale (with 5 being the highest quality). For unbiased evaluation, the readers were blinded to the patients' personal details and clinical and laboratory information as well as the reconstruction method that had
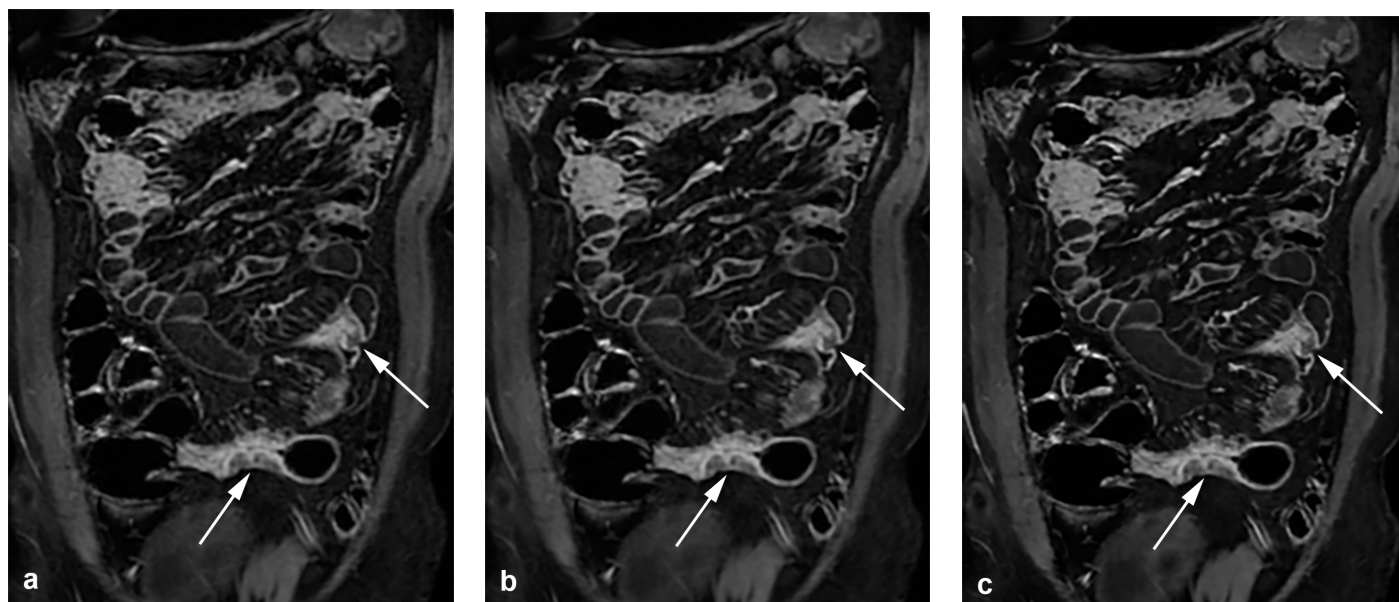

Figure 1. Dynamic enteric phase contrast-enhanced T1-weighted images of a 30-year-old man with active Crohn's disease. Three sets of coronal images were obtained, each with **(a)** conventional reconstruction and no image filter (original); **(b)** with conventional reconstruction and image filter (filtered); and **(c)** with deep-learning reconstruction (DLR) at the noise-reduction level of 75% (DLR). The DLR image **(c)** shows increased sharpness of bowel walls and mesenteric vessels, enabling better visualization of active inflammation of bowel segments and adjacent comb signs (arrows). A reduction of noise with a slight synthetic appearance is also noted in the DLR image **(c)** compared with the other two images **(a, b).**
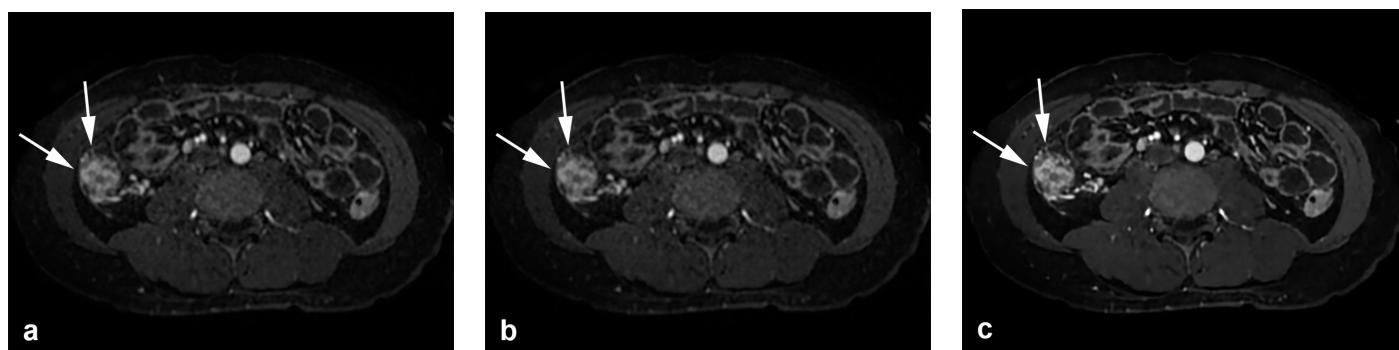

Figure 2. Dynamic enteric phase contrast-enhanced T1-weighted images of an 18-year-old man with active Crohn's disease. Three sets of images were obtained and reformatted in the axial plane with a 1.4-mm slice thickness: **(a)** with conventional reconstruction and no image filter (original); **(b)** with conventional reconstruction and image filter (filtered); and **(c)** with deep-learning reconstruction (DLR) at the noise-reduction level of 75% (DLR). The DLR image **(c)** better visualizes active inflammation in the ascending colon (arrows) with lower noise, a sharper margin of the bowel wall and vascularity, and better contrast of bowel wall stratification compared with the other two images **(a, b).** In the qualitative analysis, the DLR image was given a higher score (4 or 5) by two readers regarding overall image quality, contrast, sharpness, motion artifacts, and blurring than the other two images. The consecutive images of the same patient are also presented in Supplementary Video 1, available in the online supplement.

been applied. The analysis involved two separate image sessions without intervals: one for coronal images and the other for axial images. Blinding the image sets based on whether they were axial or coronal was not possible, and including an interval between the image sessions was deemed unnecessary, as no significant bias was likely to be generated as a result. In this qualitative analysis session, overall image quality, contrast, sharpness, presence of motion artifacts, blurring, and synthetic appearance were evaluated based on a previous study.[12] The overall image quality affecting diagnostic confidence was graded as follows: 1 = very poor image quality displaying non-diagnostic images; 2 = poor image quality with significantly impaired diagnostic confidence; 3 = fair image quality with slightly impaired diagnostic confidence; 4 = good image quality; and 5 = perfect image quality. The contrast and sharpness of the bowel walls, mesenteric vessels, and perienteric structures were evaluated analogously to the scales of overall image quality as follows: 1 = very poor contrast or sharpness with no detectable structures; 2 = poor contrast or sharpness rendering difficulty in distinguishing structures; 3 = fair contrast or sharpness with partially indistinguishable structures; 4 = good contrast or sharpness; and 5 = excellent contrast or sharpness. Motion artifacts, blurring of fine details, and synthetic appearance that could degrade image quality were rated as follows: 1 = severe artifacts or diagnostically unusable; 2 = substantial artifacts with major diagnostic impairment; 3 = moderate artifacts with minor diagnostic impairment; 4 = minimal artifacts; and 5 = no artifacts. Both blurring and synthetic appearance are artifacts that may occur with the CS technique and, potentially, with DLR.[19-21] Synthetic appearance refers to a "plastic" or "cartoon-like" appearance that is attributed to various iterative reconstructions.[20,21]

The radiologists were additionally asked to record the presence of any extramural complications in the small or large bowels (e.g., abscess, sinus tract, fistula, or inflammatory mass) and whether reviewing the reformatted axial images in addition to the coronal images was more helpful in detecting and evaluating penetrating disease than reviewing the coronal images alone.

For the quantitative image analysis, three representative locations were chosen in the coronal and axial planes (Supplementary Figure 3). For the coronal plane, images showing both the external iliac and femoral arteries at the level where multiple small bowel loops are visible, aortic bifurcation, and kidneys at the level where the ascending and descending colons are visible were chosen to calculate the SNR in the anterior, middle, and posterior portions of the abdominal cavity, respectively. For the axial plane, images at the level of the superior mesenteric artery, aortic bifurcation, and pelvic cavity showing superior gluteal veins were chosen to calculate the SNR in the upper, middle, and lower portions of the abdominal cavity, respectively. The SNR was calculated by dividing the mean signal of the slice by the estimated noise levels given in the standard deviations.[22] The noise levels were estimated using a hybrid discrete wavelet transform and edge information removal-based algorithm, which assumes that the energy of noise is equally distributed in sub-bands of wavelet coefficients but the energy of an image is mostly confined in low-low, low-high, and high-low sub-bands (Supplementary Figure 4).[23] We implemented the method using NumPy, pydicom, cv2, and pywt packages in Python (version 3.7.9).

Statistical analysis

In the qualitative analysis, mean scores for overall image quality, contrast, sharpness and presence of motion artifacts, blurring, and synthetic appearance in the three image sets measured by the two readers were compared using Friedman's test in the axial and coronal planes, respectively. If there was any significant difference between the three image groups, Bonferroni corrections were applied for multiple comparisons. The interobserver agreement of each score between the two readers was evaluated using quadratic weighted kappa coefficients. The kappa estimate was considered poor for κ < 0.21, fair for κ = 0.21–0.40, moderate for κ = 0.41–0.60, good for κ = 0.61–0.80, and excellent for κ = 0.81–1.00.[24] As the MRI images analyzed in this study were primarily used in real clinical practice, it was relatively unlikely that they were non-diagnostic images with very low-quality scores, of which the data distribution might be highly consistent and deviated. Therefore, when the weighted kappa values were not estimable because the data distribution of scores was too skewed, the overall proportion of agreement was calculated.[25,26] In the quantitative analysis, a repeated-measures analysis of variance with a Greenhouse–Geisser correction was used to compare SNRs between the three image sets. For data with a non-normal distribution, the Friedman test was performed, and the Shapiro–Wilk test was used to check if a variable followed a normal distribution. Bonferroni's method was applied in the post-hoc test. All statistical analyses were performed using SPSS version 25.0 (IBM Corp.) and Med-Calc version 18 (MedCalc Software) software. Statistical significance was set at a value of $P < 0.05$.

Results

Patient characteristics

The characteristics of the study population are summarized in Supplementary Table 1. Four patients had a history of bowel surgery due to CD complications. The mean scan time was 15.86 ± 1.14 seconds (range: 14–18 seconds).

Qualitative image analysis

The results of the qualitative image analysis, which were expressed as the mean and standard deviation of the two readers' scores, are summarized in Table 2. The results of multiple comparisons among the three image sets are presented in Supplementary Table 2. The mean scores of the DLR image set with respect to overall image quality, contrast, sharpness, motion artifacts, and blurring in both the coronal and axial images were significantly superior to those of both the filtered and original images ($P < 0.001$). However, the mean scores for synthetic appearance in DLR were significantly lower than those of the filtered and original images ($P < 0.05$). The filtered images tended to score slightly higher than the original images for overall image quality, contrast, sharpness, motion artifacts, and blurring, although they were slightly lower for synthetic appearance; however, there was no statistically significant difference between their mean scores ($P > 0.05$) (Figures 1-3, and Supplementary Figure 5 and Supplementary Video 1, available in the online supplement).

The interobserver agreement for the overall image quality, contrast, sharpness, motion artifacts, and blurring in both the coronal and axial images was moderate to excellent (κ, 0.426–1.000); however, the blurring of the axial images showed fair agreement (κ = 0.398) (Table 3). The interobserver agreement for a synthetic appearance on the coronal and axial DLR images was also good to excellent (κ, 0.660–0.828). Since the interobserver agreement for synthetic appearance in both the original and filtered images was not estimable, the overall proportion of agreement was calculated: there was no discrepancy in the coronal and axial original images and

the axial filtered images (100% agreement), and there were four discrepancies out of 35 patients (88.6% agreement) in the coronal filtered images.

Presence of extramural complications

Both readers detected extramural complications in 10 patients. There was no discordant interpretation of the presence of extramural complication between the two readers. These findings were demonstrated in the images of both the coronal and axial planes (Figure 3 and Supplementary Figure 6). Among the cases of extramural complications, the readers found that reviewing axial images in addition to coronal images was more helpful than reviewing coronal images alone in all cases (Supplementary Figure 6 and Supplementary Video 2, available in the online supplement).

Quantitative image analysis

The SNRs of the three different locations in both the coronal and axial planes were significantly increased in the order of original, filtered, and DLR images ($P < 0.001$) (Table 4). The mean SNRs of all three different locations were also compared between the three image sets in each coronal and axial plane. As a result, the mean SNR of the DLR measured was the highest, and the mean SNR of the original images was the lowest ($P < 0.001$) (Table 4).

Discussion

Our results demonstrated that the vendor-supplied prototype DLR significantly increased the SNR; improved the image quality, contrast, and sharpness; and decreased perceived motion artifacts in the enhanced T1W MRE images. Furthermore, using DLR enables high-resolution near-isotropic CE-T1W MRE with sufficient image quality. It allows high-quality axial reformatted images to be obtained from the same dynamic phase, which helps depict the anatomic details of bowel segments or extramural complications, such as fistulas or abscesses.

The CE-T1W sequence is important for evaluating active inflammation in CD.[8-10] With the advantage of rapid acquisitions, the 3D-GRE sequence is the SOC technique for CE-T1W MRE. However, this sequence is susceptible to motion artifacts, as obtaining high-resolution CE-T1W MRE within one breath hold could be challenging due to bowel peristalsis, respiration, and limited breath holding. To overcome this challenge, several approaches have been used to accelerate MRI, such as parallel imaging and CS.[13] However, excessive acceleration can cause a loss of SNR, which leads to reduced image quality.[14,27]

Recent advances in DLR offer an additional way to improve image quality and shorten the scan time. To date, the current published reports on DLR for 3D-GRE are limited in diversity. One introduced algorithm combines super resolution (Siemens) with partial Fourier reconstruction.[28,29] The algorithm is trained to perform both up-sampling in the phase-encoding direction and partial fourier reconstruction. This technique showed a significant noise reduction and improvement of image sharpness and lesion conspicuity in abdominal MRI. In our study, we used the AIR™ Recon DL (GE Healthcare) technique on 3D LAVA with CS sequences to reduce noise and ringing in all three directions.

Table 2. Qualitative analysis of the contrast-enhanced T1-weighted images of magnetic resonance enterography with three different reconstruction methods

	Original	Filtered	DLR	P value*
Coronal				
Overall image quality	3.56 ± 0.54	3.77 ± 0.56	4.67 ± 0.51	<0.001†
Contrast	3.96 ± 0.39	4.11 ± 0.46	4.69 ± 0.49	<0.001†
Sharpness	3.57 ± 0.50	3.81 ± 0.49	4.69 ± 0.50	<0.001†
Motion artifacts	3.67 ± 0.70	3.74 ± 0.79	4.33 ± 0.72	<0.001†
Blurring	3.56 ± 0.53	3.70 ± 0.49	4.24 ± 0.43	<0.001†
Synthetic appearance	5.00 ± 0.00	4.94 ± 0.16	4.44 ± 0.48	<0.001†
Axial				
Overall image quality	3.29 ± 0.47	3.59 ± 0.54	4.67 ± 0.53	<0.001†
Contrast	3.90 ± 0.34	3.90 ± 0.27	4.71 ± 0.41	<0.001†
Sharpness	3.17 ± 0.38	3.51 ± 0.49	4.64 ± 0.46	<0.001†
Motion artifacts	3.64 ± 0.59	3.66 ± 0.60	4.34 ± 0.68	<0.001†
Blurring	3.14 ± 0.38	3.46 ± 0.48	4.16 ± 0.34	<0.001†
Synthetic appearance	5.00 ± 0.00	5.00 ± 0.00	4.43 ± 0.46	<0.001†

Data are presented as mean ± standard deviation. *P values were obtained by comparing three different reconstruction methods using the Friedman test. †Post-hoc Bonferroni's test for multiple comparisons revealed significant differences between original and DLR images and between filtered and DLR images ($P < 0.05$) but not between the original and filtered images (Supplementary Table 2). Original, conventional reconstruction with no image filter; filtered, conventional reconstruction with image filter; DLR, deep-learning reconstruction.

Table 3. Interobserver agreement between the two readers for qualitative analysis

	Original	Filtered	DLR
	Kappa (95% CI)	Kappa (95% CI)	Kappa (95% CI)
Coronal			
Overall image quality	0.859 (0.694–1.000)	0.759 (0.573–0.944)	0.846 (0.660–1.000)
Contrast	0.615 (0.304–0.927)	0.650 (0.380–0.920)	0.687 (0.504–0.870)
Sharpness	0.792 (0.619–0.965)	0.731 (0.532–0.930)	0.791 (0.645–0.937)
Motion artifacts	0.760 (0.623–0.898)	0.791 (0.678–0.905)	0.867 (0.747–0.986)
Blurring	0.766 (0.553–0.980)	0.579 (0.386–0.773)	0.672 (0.433–0.910)
Synthetic appearance	N/E	N/E	0.828 (0.644–1.000)
Axial			
Overall image quality	0.673 (0.412–0.934)	0.857 (0.689–1.000)	0.949 (0.846–1.000)
Contrast	0.531 (0.165–0.896)	0.481 (0.090–0.873)	0.595 (0.325–0.865)
Sharpness	0.426 (0.050–0.802)	0.692 (0.483–0.901)	0.815 (0.618–1.000)
Motion artifacts	0.811 (0.668–0.953)	0.784 (0.635–0.933)	0.882 (0.765–0.999)
Blurring	0.525 (0.164–0.886)	0.598 (0.376–0.819)	0.398 (0.072–0.724)
Synthetic appearance	N/E	N/E	0.660 (0.427–0.893)

Original, conventional reconstruction with no image filter; filtered, conventional reconstruction with image filter; DLR, deep-learning reconstruction; N/E, not estimable; CI, confidence interval.

Table 4. Comparison of signal-to-noise ratio between the contrast-enhanced T1-weighted images of magnetic resonance enterography with three different reconstruction methods

	Original	Filtered	DLR	P value
Coronal				
Total*	52.50 ± 8.85	64.85 ± 10.95	86.15 ± 12.96	<0.001[†]
Anterior	55.10 ± 10.38	68.02 ± 12.85	87.87 ± 18.55	<0.001[†]
Middle	57.25 ± 10.96	70.78 ± 13.58	94.68 ± 15.45	<0.001[†]
Posterior	45.16 ± 6.87	55.76 ± 8.52	75.88 ± 9.43	<0.001[‡]
Axial				
Total*	49.59 ± 6.79	59.23 ± 8.12	85.19 ± 12.32	<0.001[†]
Upper	67.64 ± 13.98	80.04 ± 16.74	116.95 ± 26.25	<0.001[†]
Middle	32.74 ± 3.83	39.96 ± 4.77	62.04 ± 9.65	<0.001[‡]
Lower	48.40 ± 7.02	57.69 ± 8.51	76.58 ± 9.60	<0.001[†]

[†]P value was obtained by comparing three different reconstruction methods using repeated-measures analysis of variance with a Greenhouse–Geisser correction. Post-hoc Bonferroni's tests for multiple comparisons revealed a significant difference between the original and DLR, between the filtered and DLR, and between the original and filtered images (P < 0.05). [‡]P value was obtained by comparing three different reconstruction methods using the Friedman test. Post-hoc Bonferroni's tests for multiple comparisons revealed a significant difference between the original and DLR, between the filtered and DLR, and between the original and filtered images (P < 0.05). *Mean values of three different locations in each image set. Data are presented as mean ± standard deviation. Original, conventional reconstruction with no image filter; filtered, conventional reconstruction with image filter; DLR, deep-learning reconstruction.

The technique applies a CNN in the image reconstruction pipeline using raw k-space data. The AIR™ Recon DL technique enables the acquisition time to be reduced without affecting the image quality and high-resolution images to be obtained without reducing the SNR. We obtained high-resolution near-isotropic CE-T1W MRE images within a single breath hold and achieved sufficient image quality with the aid of CS and DLR. To our knowledge, this is the first study to evaluate the utility of DLR for 3D LAVA with CS for MRE in clinical practice.

In addition, these benefits are not restricted to the acquired imaging plane but are effective in the reformatted planes. With DLR, the SNR and image quality were improved not only in the plane but also through the plane. This can be particularly useful for improving the quality of reformatted images in clinical situations when multiple review planes can be helpful but simultaneous acquisition is required because of the time-dependent image contrast.
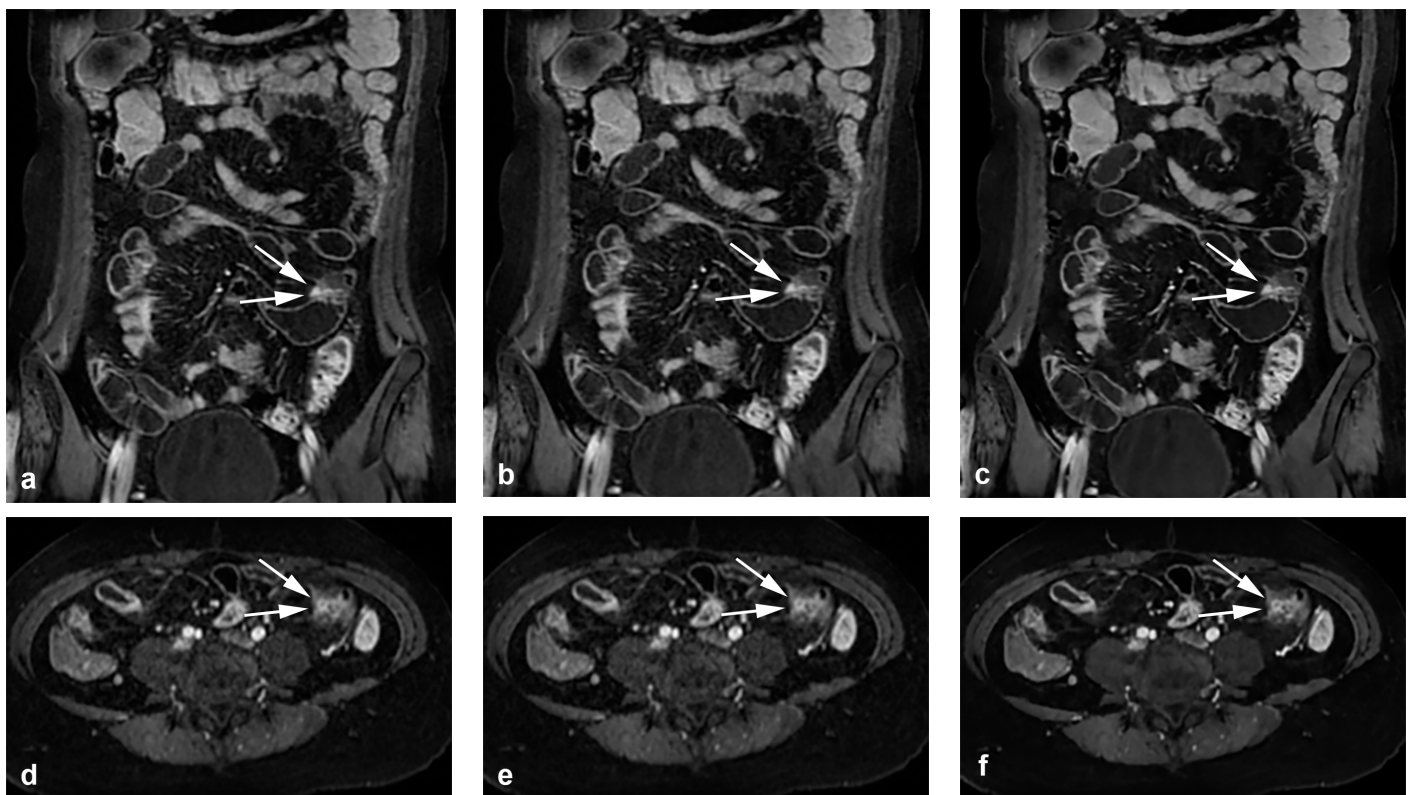

Figure 3. Dynamic enteric phase contrast-enhanced T1-weighted images of a 28-year-old woman with active Crohn's disease. Three sets of images were obtained, each with **(a)** conventional reconstruction and no image filter (original); **(b)** with conventional reconstruction and image filter (filtered); and **(c)** with deep-learning reconstruction (DLR) at the noise-reduction level of 75% (DLR). Axial images with a 1.4-mm slice thickness were reformatted from coronal images, respectively **(d-f)**. The DLR images in both the coronal and axial planes **(c,f)** show lower noise, a sharper margin of the bowel wall and vascularity, and better contrast of bowel wall stratification than the other two images **(a, b, d, e)**. In the coronal image sets, a small sinus tract is detected in the proximal ileum (arrows), which is better visualized in the DLR image **(c)**. The corresponding penetrating lesion in the proximal ileum is also well visualized in the sets of axial images (arrows) and is most clearly visible in DLR **(f)**, which helps increase diagnostic confidence.

Previously, we obtained CE-T1W images in the delayed phase after acquiring dynamic coronal T1W images. Delayed-phase axial images may help differentiate fibrosis from active inflammation.[30] However, as the bowel wall enhancement pattern and mesenteric vascularity indicative of active inflammation are most well depicted in earlier phases of the dynamic study,[31] axial images in the delayed phase could limit the provision of detailed anatomic structures and hinder lesion detection and diagnosis due to its different and non-simultaneous acquisition timing compared with that of coronal dynamic images. Our axial-reformatted CE-T1W images of the simultaneous dynamic phase of the coronal images are superior to axial CE-T1W images of the delayed phase for evaluating active inflammation. Also, axial images help detect penetrating complications, such as fistulas and abscesses, by multiplanar correlation.[30] In our study, both readers stated that an additional review of the axial images was helpful in the detection and evaluation of penetrating disease in all cases. In addition, because we can obtain axial images without additional image acquisition, we can reduce the total scan time of MRE. Although the acquisition time of additional axial images is quite short, a shorter scan time is better for patient compliance because the oral administration of polyethylene glycol can cause the urge to evacuate during MR acquisition.

Our study has several limitations. First, the images were retrospectively reviewed. Second, the sample size was relatively small. Third, although we conducted a blinded analysis for each image set, the significant reduction in noise and the differences in image texture made perfect blinding impossible. Fourth, in our study, the generation of images with DLR took a relatively significant length of time, approximately one hour for each series, due to the computational intensity of the DLR technique. While this process could be accelerated significantly using graphics processing units, the long reconstruction time could be a drawback for using DLR in real practice. Nonetheless, this technique is currently available commercially and has been integrated into the hardware of MR machines; the reconstruction is generated immediately after image acquisition and is displayed almost simultaneously with the original image. Fifth, we acknowledge that our study's inclusion of only patients with CD, who tend to be young with a low body mass index, may limit the generalizability of our study results to the broader population. Further, we did not statistically analyze the

detection of penetrating disease in the axial reformatted images. The number of cases of penetrating disease was small, and penetrating disease could already be detected with coronal images. However, both readers mentioned that additional axial images could help increase their diagnostic confidence in all cases. Finally, we did not evaluate the diagnostic accuracy for active inflammation. Our study aimed to assess the image quality of near-isotropic CE-T1W MRE using DLR. Previous studies[8,10,12,30,31] used endoscopic findings or findings from full-protocol MRE as the reference standard for active inflammation in CD. In our study, we compared the image quality between image sets obtained from the same image scan with different reconstructions. MRE has demonstrated high diagnostic performance for the diagnosis of active inflammation in CD.[32,33] We believe that comparing diagnostic performance between image sets from the same scan image, which is already used in real clinical practice, is not essential. Furthermore, CE-T1W images play the most important role in evaluating active inflammation among the multiple sequences of MRE. Therefore, we considered that reference from full-protocol MRE was inappropriate in our study because the CE-T1W used as a reference standard was the same image as the image sets to be compared.

In conclusion, this is the first study to investigate DLR for CE-T1W MRE in clinical practice. The use of DLR for near-isotropic CE-T1W MRE provides improved image quality and an increased SNR. It allows high-quality axial reformatted images to be obtained from the same dynamic phase, which is useful for the multiplanar evaluation of anatomical details of bowel segments or extramural complications.

Conflict of interest disclosure

The authors declared no conflicts of interest.

Funding

References

1. Lichtenstein GR, Loftus EV, Isaacs KL, Regueiro MD, Gerson LB, Sands BE. ACG clinical guideline: management of Crohn's disease in adults. *Am J Gastroenterol*. 2018;113(4):481-517. Erratum in: *Am J Gastroenterol*. 2018;113(7):1101. [CrossRef]

2. Reinisch S, Schweiger K, Pablik E, et al. An index with improved diagnostic accuracy for the diagnosis of Crohn's disease derived from the Lennard-Jones criteria. *Aliment Pharmacol Ther*. 2016;44(6):601-611. [CrossRef]

3. Kim SC, Ferry GD. Inflammatory bowel diseases in pediatric and adolescent patients: clinical, therapeutic, and psychosocial considerations. *Gastroenterology*. 2004;126(6):1550-1560. [CrossRef]

4. Park SH, Kim YJ, Rhee KH, et al. A 30-year trend analysis in the epidemiology of inflammatory bowel disease in the Songpa-Kangdong District of Seoul, Korea in 1986-2015. *J Crohns Colitis*. 2019;13(11):1410-1417. [CrossRef]

5. Horsthuis K, Bipat S, Stokkers PC, Stoker J. Magnetic resonance imaging for evaluation of disease activity in Crohn's disease: a systematic review. *Eur Radiol*. 2009;19(6):1450-1460. [CrossRef]

6. Messaris E, Chandolias N, Grand D, Pricolo V. Role of Magnetic resonance enterography in the management of Crohn disease. *Arch Surg*. 2010;145(5):471-475. [CrossRef]

7. Tolan DJ, Greenhalgh R, Zealley IA, Halligan S, Taylor SA. MR enterographic manifestations of small bowel Crohn disease. *RadioGraphics*. 2010;30(2):367-384. [CrossRef]

8. Low RN, Sebrechts CP, Politoske DA, et al. Crohn disease with endoscopic correlation: single-shot fast spin-echo and gadolinium-enhanced fat-suppressed spoiled gradient-echo MR imaging. *Radiology*. 2002;222(3):652-660. [CrossRef]

9. Pupillo VA, Di Cesare E, Frieri G, Limbucci N, Tanga M, Masciocchi C. Assessment of inflammatory activity in Crohn's disease by means of dynamic contrast-enhanced MRI. *Radiol Med*. 2007;112(6):798-809. [CrossRef]

10. Spieler B, Hindman N, Levy J, et al. Contrast-enhanced MR enterography as a stand-alone tool to evaluate Crohn's disease in a paediatric population. *Clin Radiol*. 2013;68(10):1024-1030. [CrossRef]

11. Tongdee R, Narra VR, Oliveira EP, Chapman W, Elsayes KM, Brown JJ. Utility of 3D magnetic resonance imaging in preoperative evaluation of hepatobiliary diseases. *HPB (Oxford)*. 2006;8(4):311-317. [CrossRef]

12. Kim J, Seo N, Bae H, et al. Comparison of Sensitivity Encoding (SENSE) and compressed sensing-SENSE for contrast-enhanced T1-weighted imaging in patients with Crohn disease undergoing MR enterography. *AJR Am J Roentgenol*. 2022;218(4):678-686. [CrossRef]

13. Yoon JH, Nickel MD, Peeters JM, Lee JM. Rapid imaging: recent advances in abdominal MRI for reducing acquisition time and its clinical applications. *Korean J Radiol*. 2019;20(12):1597-1615. [CrossRef]

14. Kale SC, Chen XJ, Henkelman RM. Trading off SNR and resolution in MR images. *NMR Biomed*. 2009;22(5):488-494. [CrossRef]

15. Ueda T, Ohno Y, Yamamoto K, et al. Compressed sensing and deep learning reconstruction for women's pelvic MRI denoising: utility for

improving image quality and examination time in routine clinical practice. *Eur J Radiol*. 2021;134:109430. [CrossRef]

16. Lebel RM. Performance characterization of a novel deep learning-based MR image reconstruction pipeline. arXiv. 2020. [CrossRef]

17. Sun S, Tan ET, Mintz DN, et al. Evaluation of deep learning reconstructed high-resolution 3D lumbar spine MRI. *Eur Radiol*. 2022;32(9):6167-6177. [CrossRef]

18. Chazen JL, Tan ET, Fiore J, Nguyen JT, Sun S, Sneag DB. Rapid lumbar MRI protocol using 3D imaging and deep learning reconstruction. *Skeletal Radiol*. 2023. [CrossRef]

19. Jaspan ON, Fleysher R, Lipton ML. Compressed sensing MRI: a review of the clinical literature. *Br J Radiol*. 2015;88(1056):20150487. [CrossRef]

20. Shaikh J, Stoddard PB, Levine EG, et al. View-sharing artifact reduction with retrospective compressed sensing reconstruction in the context of contrast-enhanced liver MRI for hepatocellular carcinoma (HCC) screening. *J Magn Reson Imaging*. 2019;49(4):984-993. [CrossRef]

21. Zhang T, Chowdhury S, Lustig M, et al. Clinical performance of contrast enhanced abdominal pediatric MRI with fast combined parallel imaging compressed sensing reconstruction. *J Magn Reson Imaging*. 2014;40(1):13-25. [CrossRef]

22. Dietrich O, Raya JG, Reeder SB, Reiser MF, Schoenberg SO. Measurement of signal-to-noise ratios in MR images: influence of multichannel coils, parallel imaging, and reconstruction filters. *J Magn Reson Imaging*. 2007;26(2):375-385. [CrossRef]

23. Pimpalkhute VA, Page R, Kothari A, Bhurchandi KM, Kamble VM. Digital image noise estimation using DWT coefficients. *IEEE Trans Image Process*. 2021;30:1962-1972. [CrossRef]

24. Landis JR, Koch GG. The measurement of observer agreement for categorical data. *Biometrics*. 1977;33(1):159-174. [CrossRef]

25. Kundel HL, Polansky M. Measurement of observer agreement. *Radiology*. 2003;228(2):303-308. [CrossRef]

26. Llewellyn A, Whittington C, Stewart G, Higgins JP, Meader N. The use of Bayesian Networks to assess the quality of evidence from research synthesis: 2. inter-rater reliability and comparison with standard GRADE assessment. *PLoS One*. 2015;10(12):e0123511. [CrossRef]

27. Yang RK, Roth CG, Ward RJ, deJesus JO, Mitchell DG. Optimizing abdominal MR imaging: approaches to common problems. *Radiographics*. 2010;30(1):185-199.[CrossRef]

28. Almansour H, Herrmann J, Gassenmaier S, et al. Combined deep learning-based super-resolution and partial fourier reconstruction for gradient echo sequences in abdominal MRI at 3 Tesla: shortening breath-hold time and improving image sharpness and lesion conspicuity. *Acad Radiol*. 2022:S1076-6332(22)00327-0. [CrossRef]

29. Wessling D, Herrmann J, Afat S, et al. Application of a deep learning algorithm for combined super-resolution and partial fourier reconstruction including time reduction in T1-weighted precontrast and postcontrast gradient echo imaging of abdominopelvic MR imaging. *Diagnostics (Basel)*. 2022;12(10):2370. [CrossRef]

30. Gee MS, Nimkin K, Hsu M, et al. Prospective evaluation of MR enterography as the primary imaging modality for pediatric Crohn disease assessment. *AJR Am J Roentgenol*. 2011;197(1):224-231. [CrossRef]

31. Del Vescovo R, Sansoni I, Caviglia R, et al. Dynamic contrast enhanced magnetic resonance imaging of the terminal ileum: differentiation of activity of Crohn's disease. *Abdom Imaging*. 2008;33(4):417-424. [CrossRef]

32. Church PC, Turner D, Feldman BM, et al. Systematic review with meta-analysis: magnetic resonance enterography signs for the detection of inflammation and intestinal damage in Crohn's disease. *Aliment Pharmacol Ther*. 2015;41(2):153-166. [CrossRef]

33. Qiu Y, Mao R, Chen BL, et al. Systematic review with meta-analysis: magnetic resonance enterography vs. computed tomography enterography for evaluating disease activity in small bowel Crohn's disease. *Aliment Pharmacol Ther*. 2014;40(2):134-146. [CrossRef]

**Supplementary Table 1.** Demographics and Crohn's disease-related characteristics of the study population

Characteristics	Value
Age (years)*	31.8 ± 10.2 (16–51)
Sex	
Male	19 (54.3)
Female	16 (45.7)
Anthropometric data[†]	
Height (cm)	167.0 (159.7–175.8)
Weight (kg)	59.0 (51.7–69.0)
BMI (kg/m²)	21.5 (19.1–23.3)
Laboratory data[†]	
Fecal calprotectin (mg/kg)	300.0 (82.0–858.0)
CRP (mg/dL)	0.13 (0.05–0.37)
Patients with previous bowel surgery	4 (11.4)

*Data are expressed as mean ± standard deviation, with ranges in parentheses. [†]Data are expressed as median, with interquartile range in parentheses. Unless otherwise specified, the data are numbers of patients, with percentages in parentheses. BMI, body mass index; CRP, C-reactive protein.

Supplementary Table 2. Results of the post-hoc Bonferroni's test for multiple comparisons among three different reconstruction methods in the qualitative analysis of the contrast-enhanced T1-weighted images of magnetic resonance enterography

|	Original vs. DLR	Filtered vs. DLR	Original vs. filtered
Coronal			
Overall image quality	<0.001	<0.001	0.51
Contrast	<0.001	<0.001	0.77
Sharpness	<0.001	<0.001	0.36
Motion artifacts	<0.001	<0.001	1.00
Blurring	<0.001	<0.001	0.85
Synthetic appearance	<0.001	0.003	1.00
Axial			
Overall image quality	<0.001	<0.001	0.28
Contrast	<0.001	<0.001	1.00
Sharpness	<0.001	<0.001	0.08
Motion artifacts	<0.001	<0.001	1.00
Blurring	<0.001	<0.001	0.06
Synthetic appearance	<0.001	<0.001	1.00

Data are presented as *P* values. Original, conventional reconstruction with no image filter; filtered, conventional reconstruction with image filter; DLR, deep-learning reconstruction.
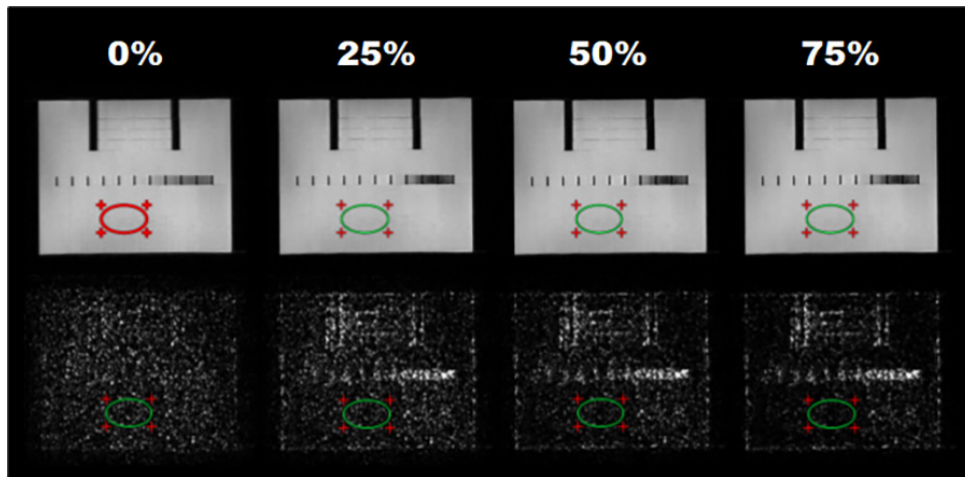
Supplementary Figure 1. The phantom experiments to evaluate the effects of different levels of noise reduction on deep-learning reconstruction (DLR). Phantom magnetic resonance images were processed using the prototype DLR with tunable noise-reduction factors of 0%, 25%, 50%, and 75%. As the noise-reduction levels increased, the signal-to-noise ratio calculated by placing a region of interest in each phantom image improved by 61.9, 66.6, 77.5, and 91.8.
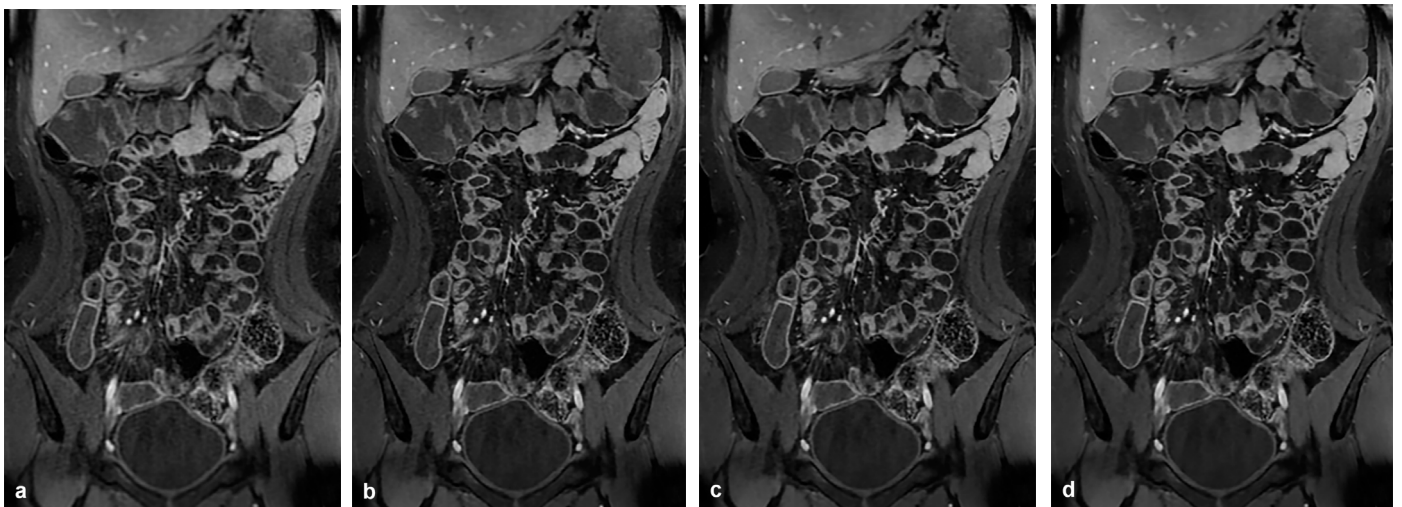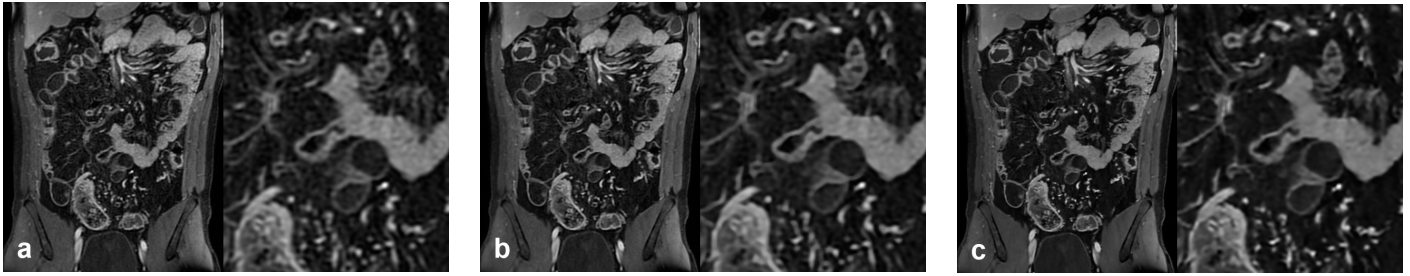

Supplementary Figure 2. The coronal images of dynamic enteric phase contrast-enhanced T1-weighted magnetic resonance enterography processed using deep-learning reconstruction (DLR) with different noise-reduction factors of **(a)** 0%, **(b)** 25%, **(c)** 50%, and **(d)** 75%. During preliminary reading sessions, the optimal denoising level was determined based on the consensus of the expert readers. The denoising level of 75% was chosen as it was found to yield the highest signal-to-noise ratio and the best image sharpness among the evaluated noise-reduction factors. Despite some synthetic appearance, it was concluded that the overall synthetic appearance produced by DLR was acceptable.
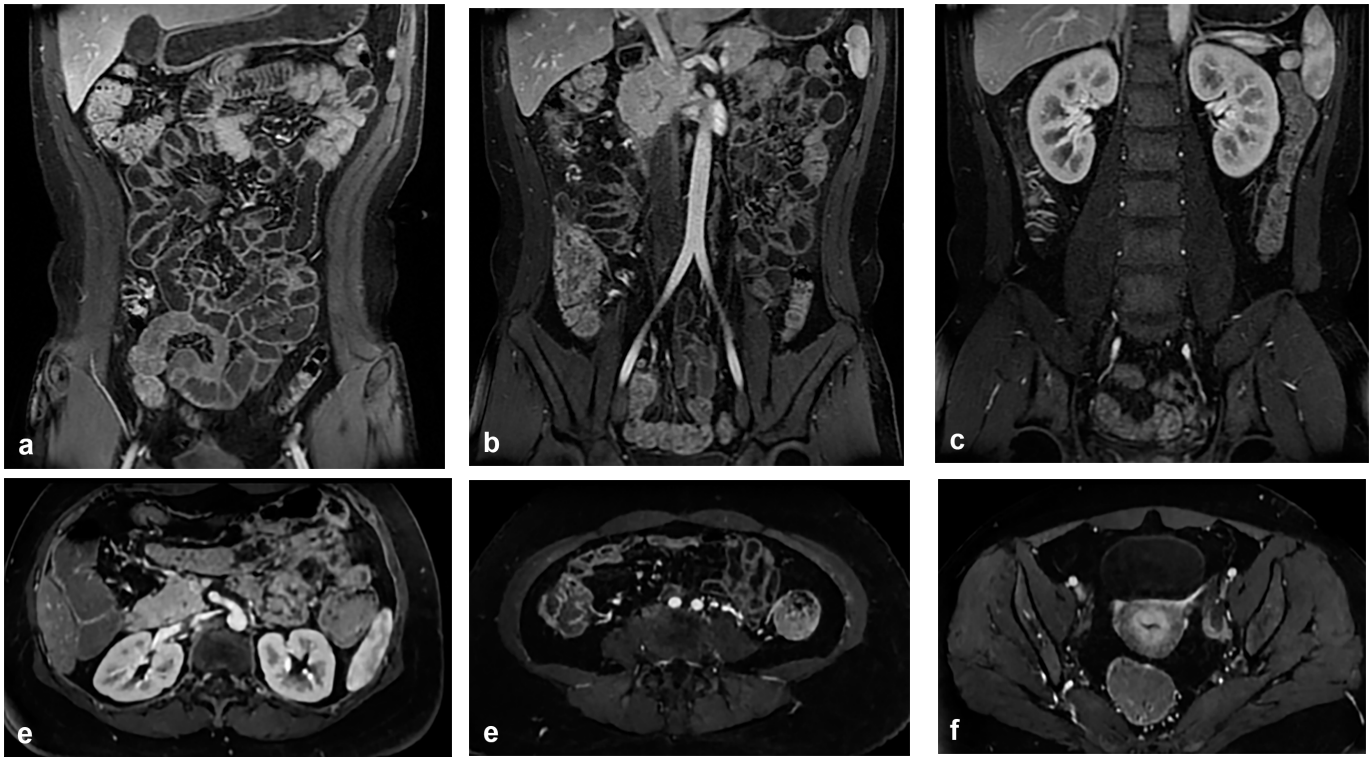
Supplementary Figure 3. Example of three representative locations selected to measure the signal-to-noise ratio (SNR) in each coronal **(a-c)** and axial **(d-f)** plane. For the coronal plane, images showing both external iliac and femoral arteries at the level where multiple small bowel loops are visible **(a)**, aortic bifurcation **(b)**, and kidneys at the level where the ascending and descending colon are visible **(c)** were chosen to calculate the SNR in the anterior, middle, and posterior portions of the abdominal cavity, respectively. For the axial plane, images at the level of **(d)** the superior mesenteric artery, **(e)** aortic bifurcation, and **(f)** the pelvic cavity showing superior gluteal veins were chosen to calculate the SNR in the upper, middle, and lower portions of the abdominal cavity, respectively.
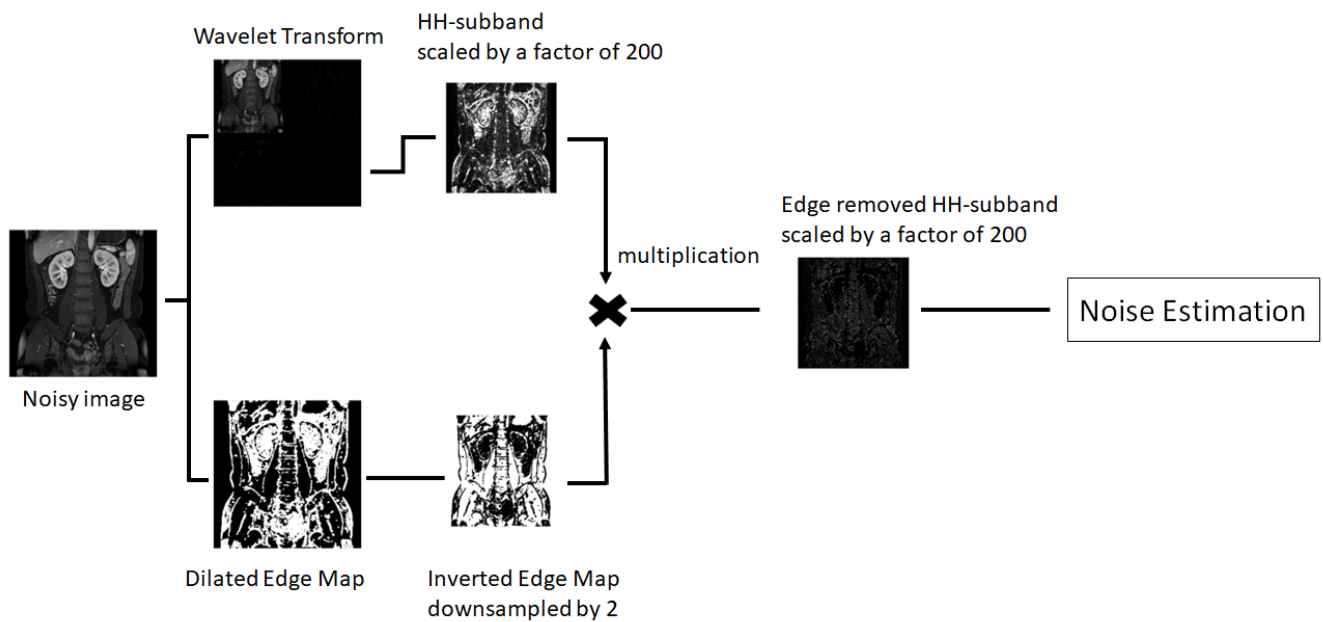
Supplementary Figure 4. Flow chart of noise estimation in a coronal image at the level of the kidneys. For the noise estimation, the modified (HH) sub-band that contains coefficients corresponding only to noise was obtained by removing the HH sub-band coefficients corresponding to edges using discrete wavelet transform and edge map.

Supplementary Figure 5. Dynamic enteric phase contrast-enhanced T1-weighted images of a 41-year-old man with active Crohn's disease. Three sets of coronal images were obtained with a 1.4-mm slice thickness: **(a)** with conventional reconstruction and no image filter (original); **(b)** with conventional reconstruction and image filter (filtered); and **(c)** with deep-learning reconstruction (DLR) at the noise-reduction level of 75% (DLR). The portion of the small bowel mesentery and bowel loops is magnified to better illustrate the structures in each image. The DLR image **(c)** demonstrates reduced noise, whereas the other two images **(a, b)** still have noise that is well visualized in the background mesenteric fat. Note that better contrast and sharpness are seen for mesenteric vessels in DLR **(c)**. However, DLR **(c)** typically demonstrates a synthetic appearance, which refers to a "plastic" or "cartoon-like" appearance.
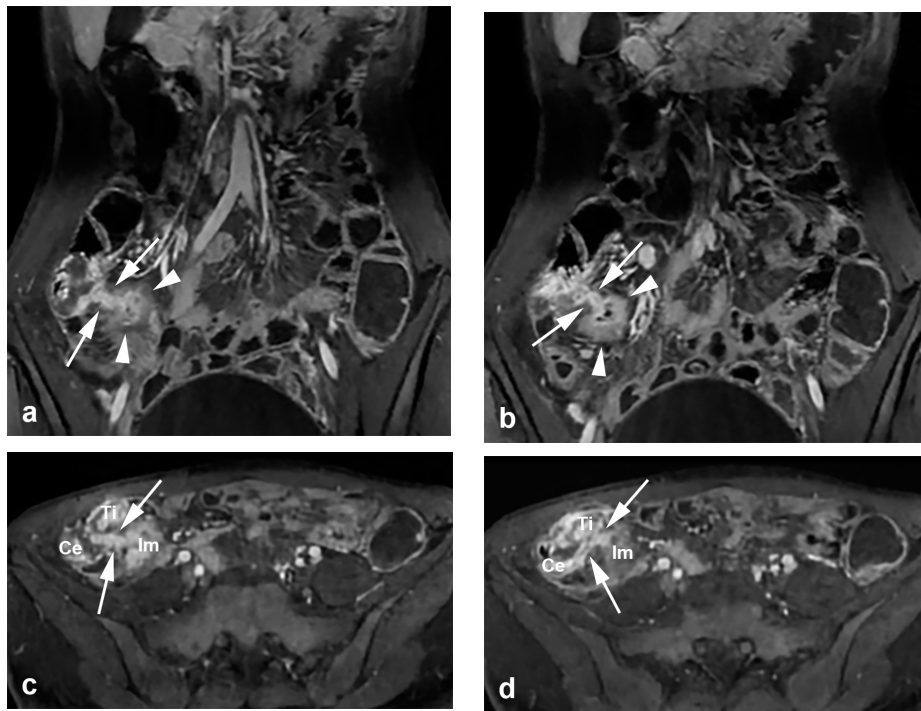
Supplementary Figure 6. Dynamic enteric phase contrast-enhanced T1-weighted images of a 27-year-old woman with active Crohn's disease. The coronal images **(a, b)** were obtained using deep-learning reconstruction at the noise-reduction level of 75% and then reformatted to axial images **(c, d)**. In the coronal images, an inflammatory mass in the ileocecal area (arrowheads) is noted with two fistulous tracts connected to the bowel loops (arrows). In the axial images, one of the fistulous tracts (arrows in a, c) reveals a connection between the inflammatory mass (Im) and the cecum (Ce), whereas the other tract (arrows in b and d) is a bidirectional fistula communicating between the cecum (Ce), terminal ileum (Ti), and inflammatory mass (Im). Two fistulas are demonstrated as more caudal to the ileocecal valve (not shown). Note that the relationship of the bidirectional fistulous tract between the bowel loops is clearly visible in the axial images, which help clarify anatomic detail when reviewed along with coronal images. The consecutive images of the same patient are also presented in Supplementary Video 2, available in the online supplement.

Supplementary Video 1 link: **(a)** https://www.youtube.com/watch?v=r2_jXqEte6Q

                                    (b) https://www.youtube.com/watch?v=7CKdrLCjhAg

                                    (c) https://www.youtube.com/watch?v=t4xtnUj0-6A

Supplementary Video 1. Videos of consecutive images from an 18-year-old man with active Crohn's disease who underwent dynamic enteric phase contrast-enhanced T1-weighted magnetic resonance enterography. Three sets of images were obtained and reformatted in the axial plane with a 1.4-mm slice thickness: **(a)** with conventional reconstruction and no image filter (original); **(b)** with conventional reconstruction and image filter (filtered); and **(c)** with deep-learning reconstruction (DLR) at the noise-reduction level of 75% (DLR). The videos were taken from all image sets at a fixed window level (2.666 HU) and width (5.320 HU). The DLR images **(c)** better visualize active inflammation in the ascending colon with lower noise, a sharper margin of the bowel wall and vascularity, and better contrast of bowel wall stratification compared with the other two images **(a, b)**. In the qualitative analysis, the DLR image was given a higher score (5) by the two readers regarding overall image quality, contrast, sharpness, and motion artifacts than the other two images (both 4). The key images of the same patient are presented in Figure 2.

Supplementary Video 2 link: **(a)** https://www.youtube.com/watch?v=reRKonWDGBM

                                    (b) https://www.youtube.com/watch?v=Qo75KqG9QI4

Supplementary Video 2. Video of consecutive images from a 27-year-old woman with active Crohn's disease who underwent dynamic enteric phase contrast-enhanced T1-weighted magnetic resonance enterography. The coronal images **(a)** were obtained using deep-learning reconstruction at the noise-reduction level of 75% and then reformatted to axial images **(b)**. In the coronal images, an inflammatory mass in the ileocecal area (Im) is noted with two fistulous tracts connected to bowel loops (red/white arrows in a). In the axial images, one of the fistulous tracts (red arrows in b) reveals a connection between the inflammatory mass and the cecum, whereas the other tract (white arrows in b) is a bidirectional fistula communicating between the cecum, the terminal ileum, and the inflammatory mass. Two fistulas are demonstrated more caudal to the ileocecal valve. Note that the relationship of the bidirectional fistulous tract between the bowel loops is clearly visible in the axial images, which help clarify anatomic detail when reviewed along with coronal images. The key images of the same patient are presented in Supplementary Figure 6.